ML-CIRRUS

THE AIRBORNE EXPERIMENT ON NATURAL CIRRUS AND CONTRAIL CIRRUS WITH THE HIGH-ALTITUDE LONG-RANGE RESEARCH AIRCRAFT HALO

The ML-CIRRUS experiment deployed the new research aircraft HALO together with satellites and models to gain new insights into nucleation, life cycle, predictability, and climate impact of natural cirrus and anthropogenic contrail cirrus.

Cloud probes on the research aicraft HALO during the ML-CIRRUS experiment

Christiane Voigt, Ulrich Schumann, Andreas Minikin, Ahmed Abdelmonem, Armin Afchine, Stephan Borrmann, Maxi Boettcher, Bernhard Buchholz, Luca Bugliaro, Anja Costa, Joachim Curtius, Maximilian Dollner, Andreas Dörnbrack, Volker Dreiling, Volker Ebert, Andre Ehrlich, Andreas Fix, Linda Forster, Fabian Frank, Daniel Fütterer, Andreas Giez, Kaspar Graf, Jens-Uwe Grooß, Silke Groß, Katharina Heimerl, Bernd Heinold, Tilman Hüneke, Emma Järvinen, Tina Jurkat, Stefan Kaufmann, Mareike Kenntner, Marcus Klingebiel, Thomas Klimach, Rebecca Kohl, Martina Krämer, Trismono Candra Krisna, Anna Luebke, Bernhard Mayer, Stephan Mertes, Sergej Molleker, Andreas Petzold, Klaus Pfeilsticker, Max Port, Markus Rapp, Philipp Reutter, Christian Rolf, Diana Rose, Daniel Sauer, Andreas Schäfler, Romy Schlage, Martin Schnaiter, Johannes Schneider, Nicole Spelten, Peter Spichtinger, Paul Stock, Adrian Walser, Ralf Weigel, Bernadett Weinzierl, Manfred Wendisch, Frank Werner, Heini Wernli, Martin Wirth, Andreas Zahn, Helmut Ziereis, and Martin Zöger

Cirrus clouds are composed of ice particles and cover about 30% of the midlatitude troposphere (Wylie and Menzel 1999). Cirrus clouds influence climate by increasing the solar albedo (cooling) and trapping thermal infrared radiation (warming). As a net effect, cirrus clouds are expected to contribute on average to a warming of Earth's atmosphere, with details depending on cirrus properties and atmospheric and Earth surface parameters (Liou 1986).

Midlatitude cirrus are induced and affected by various weather systems in a region with strong meridional gradients, land–ocean contrasts, and by natural and anthropogenic aerosol sources. Also, cirrus may feed back onto dynamics. In sum, this complexity explains why cirrus processes are still only crudely represented in today's weather predictions (Bauer et al. 2015) and why clouds including cirrus pose major uncertainties on climate sensitivity (Stevens and Bony 2013). In addition, measuring cirrus properties poses a challenge to the present day's cloud instruments, in particular as the upper troposphere–lower stratosphere (UTLS) region is difficult to access.

Midlatitude cirrus clouds can be influenced by the dense air traffic in this region (IPCC 1999). Currently, aircraft-induced condensation trails or contrail cirrus are considered to be responsible for the major part of the aviation climate impact (IPCC 2013), and growth rates in aviation (Lee et al. 2009) suggest future increases. Still, large uncertainties remain in our understanding of the microphysical properties of contrail cirrus, their occurrence, and climate effects (Heymsfield et al. 2010), which limit our ability to identify and implement proper mitigation measures to reduce the climate impact from aviation. These challenges in atmospheric research motivate the objectives of the Midlatitude Cirrus experiment (ML-CIRRUS), which are to

1) investigate distributions of microphysical and radiative properties of cirrus clouds and of humidity to better understand and more accurately quantify their climate impact,
2) study cirrus properties and lifetime in meteorological regimes typical for midlatitudes,
3) examine cirrus formation pathways and their impact on small- and large-scale cirrus properties,
4) validate satellite products and ground-based observations and evaluate advanced cloud models,
5) assess cirrus and contrail cirrus predictability, and
6) directly observe contrail cirrus and investigate differences between anthropogenic and natural cirrus.

The ML-CIRRUS campaign (www.pa.op.dlr.deML-CIRRUS) was one of the first scientific missions demonstrating the capabilities of the novel High Altitude and Long Range Research Aircraft (HALO; www.halo.dlr.de), a twin-engine jet aircraft of type Gulfstream 550, with about 10,000-km range, 14.5-km ceiling altitude, and 3,000-kg scientific payload. For ML-CIRRUS, HALO was equipped with a unique set of instruments, designed to characterize the microphysical, optical, and radiative properties of cirrus clouds and their environment. The aircraft measurements were combined with cloud data retrieved from the Spinning

Publisher's Note: This article was modified on 28 February 2017 to correct the reference Heymsfield et al. 2010.

AFFILIATIONS: Voigt—Deutsches Zentrum für Luft-und Raumfahrt, Oberpfaffenhofen, and Johannes Gutenberg-Universität, Mainz, Germany; Schumann, Minikin, Bugliaro, Dörnbrack, Dreiling, Fix, Fütterer, Giez, Graf, Groß, Heimerl, Jurkat, Kaufmann, Kenntner, Petzold,[A] Rapp, Schäfler, Schlage, Stock, Weinzierl,[B] Wirth, Ziereis, and Zöger—Deutsches Zentrum für Luft-und Raumfahrt, Oberpfaffenhofen, Germany; Abdelmonem, Järvinen, Schnaiter, and Zahn—Karlsruhe Institute of Technology, Karlsruhe, Germany; Afchine, Costa, Grooß, Krämer, Luebke, Rolf, and Spelten—Forschungszentrum Jülich, Jülich, Germany; Borrmann—Johannes Gutenberg-Universität, and Max-Planck-Institut für Chemie, Mainz, Germany; Boettcher and Wernli—Eidgenössische Technische Hochschule, Zürich, Switzerland; Buchholz and Ebert—Physikalisch-Technische Bundesanstalt, Braunschweig, Germany; Curtius, Frank, Kohl, and Rose—Goethe-Universität Frankfurt, Frankfurt am Main, Germany; Dollner, Sauer, and Walser—Ludwig-Maximilians-Universität, München, and Deutsches Zentrum für Luft-und Raumfahrt, Oberpfaffenhofen, Germany; Ehrlich, Krisna, Wendisch, and Werner[C]—Universität Leipzig, Leipzig, Germany; Forster and Mayer—Ludwig-Maximilians-Universität, München, Germany; Heinold and Mertes—Leibniz–Institut für Troposphärenforschung (TROPOS), Leipzig, Germany; Hüneke and Pfeilsticker—Ruprecht-Karls-Universität Heidelberg, Heidelberg, Germany; Klingebiel, Reuter, Spichtinger, and Weigel—Johannes Gutenberg-Universität, Mainz, Germany; Klimach, Molleker, Port, and Schneider—Max-Planck-Institut für Chemie, Mainz, Germany
[A] **CURRENT AFFILIATION:** Forschungszentrum Jülich, Jülich, Germany
[B] **CURRENT AFFILIATION:** University of Vienna, Vienna, Austria
[C] **CURRENT AFFILIATION:** Joint Center for Earth Systems Technology, Baltimore, Maryland
CORRESPONDING AUTHOR E-MAIL: Christiane Voigt, christiane.voigt@dlr.de

The abstract for this article can be found in this issue, following the table of contents.
DOI:10.1175/BAMS-D-15-00213.1

In final form 10 May 2016

Enhanced Visible and Infrared Imager (SEVIRI) aboard the Meteosat Second Generation Satellite (MSG; Schmetz et al. 2002), the Moderate Resolution Imaging Spectroradiometer (MODIS) on *Aqua* (Barnes et al. 1998), and the Cloud–Aerosol Lidar with Orthogonal Polarization (CALIOP) aboard *Cloud–Aerosol Lidar and Infrared Pathfinder Satellite Observations* (*CALIPSO*; Winker et al. 2010). In addition, ground-based stations at the Universities of Munich and Leipzig and the Research Center Jülich were overflown to complement the episodic airborne observations with continuous high-resolution measurements. Hence, capacious and detailed datasets on microphysical and optical properties of midlatitude cirrus clouds were gathered during the ML-CIRRUS experiment.

ML-CIRRUS was conducted over Europe out of Oberpfaffenhofen (48°5′N, 11°17′E) in southern Germany in March and April 2014. The location is well suited to reach cirrus over all parts of Europe and was also chosen for fast access to regions with high air traffic abundance, with more than 30,000 commercial flights over Europe per day. A mission in midlatitudes provides the unique opportunity to measure cirrus clouds linked to a large variety of dynamical weather regimes, such as frontal systems, ridges, high pressure systems, jet streams, mountain waves, and convection at HALO cruise altitudes. In particular, a case study of cirrus formation in the outflow of a warm conveyor belt (WCB) by Spichtinger et al. (2005) motivated flight planning for ML-CIRRUS. The spring season was chosen to combine a high abundance of both WCBs (Madonna et al. 2014) and contrail cirrus.

This paper describes the scientific background of ML-CIRRUS and relevant open questions, the HALO instrumentation, models used in support of experiment planning, the flight strategy, and the paths and scopes of the individual flights. Moreover, it presents highlights and selected results from the ML-CIRRUS experiment and discusses the measurements in view of current topics on cirrus research.

SCIENTIFIC BACKGROUND AND PREVIOUS RESEARCH. In contrast to liquid water clouds, cirrus clouds contain low concentrations of nonspherical ice crystals. Thin cirrus generally tend to heat the atmosphere (Liou 1986), but their radiative effect is strongly modulated by a multitude of parameters including ice crystal number, size, and complexity (Wendisch et al. 2007; Zhang et al. 1999) as well as the abundance, location, and altitude of the cirrus in the atmosphere. Altogether, the radiative impact of midlatitude cirrus is not well quantified, in particular the solar albedo effect of the ice particles is poorly constrained (Chen et al. 2000; Yang et al. 2012). In addition, cirrus clouds modulate the distribution of the greenhouse gas water vapor (Trenberth et al. 2007) and of other condensed species (e.g., nitric acid; Voigt et al. 2006). Although water vapor (besides temperature) is a

Table 1. HALO cloud particle instrumentation for ML-CIRRUS. A suite of advanced microphysical cloud probes, aerosol instruments, and a microwave temperature profiler are integrated in the HALO wing stations.

Instrument	Measured properties and range	Principal investigator (Institution)
CAS-DPOL Cloud and aerosol spectrometer	Particle size distribution, polarization, 0.6–50 μm	Minikin/Voigt/Weinzierl [Deutsches Zentrum für Luft-und Raumfahrt (DLR)]
CCP (CDP/CIP) Cloud combination probe	Particle size distribution, shape, CDP 3–50 μm; CIP 15–960 μm	Weigel/Borrmann (Uni Mainz)
NIXE–CAPS (CAS–DPOL/CIP) Cloud and aerosol spectrometer	Particle size distribution, shape, polarization, CAS 0.6–50 μm; CIP 15–960 μm	Krämer (FZ Jülich)
Particle Habit Imaging and Polar Scattering Probe (PHIPS)	Particle size distribution, phase function, 10–1,000 μm	Schnaiter/Abdelmonem [Karlsruhe Institute of Technology (KIT)]
Precipitation imaging probe (PIP)	Particle size distribution, shape, 100–6,400 μm	Weigel/Borrmann (Uni Mainz)
Passive Cavity Aerosol Spectrometer Probe (PCASP-100X)	Aerosol size distribution, 0.12–3.5 μm	Minikin/Weinzierl (DLR)
Small Ice Detector Mark 3 (SID-3)	Particle size distribution, complexity, 5–50 μm	Schnaiter (KIT)
UHSAS	Dry particle size distribution, 60–1,000 nm	Minikin/Weinzierl (DLR)
Microwave temperature profiler (MTP)	Microwave radiance at 56.363, 57.612, and 58.363 GHz for temperature profile	Kenntner/Fix (DLR)

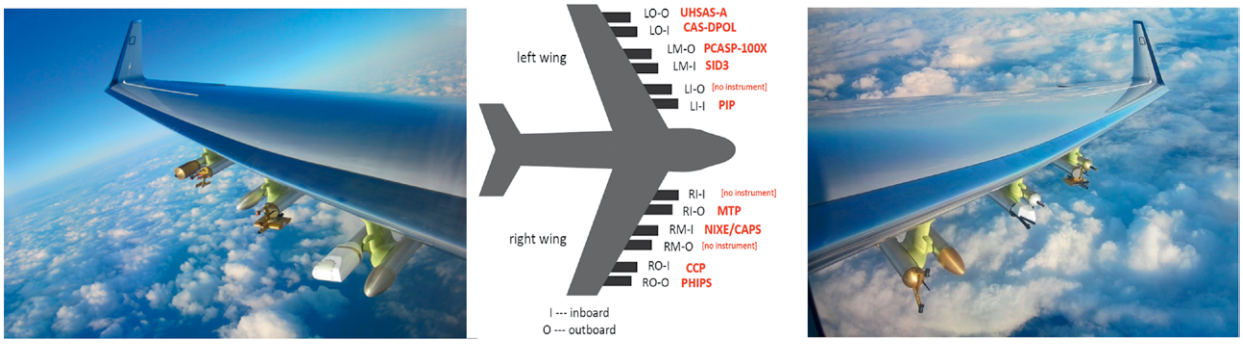

Fig. 1. Particle-measuring systems in HALO wing stations: six cloud probes, two aerosol spectrometers, and a microwave temperature profiler were integrated in the wing stations. Details of the instruments are given in Table 1.

major factor controlling cirrus formation, the accurate detection of low water vapor concentrations typical for the UTLS still presents a challenge to instrumental methods (Fahey et al. 2014). This holds even more when high temporal and spatial resolution is needed.

Cirrus formation is often induced by large-scale or mesoscale ascending atmospheric motions at midlatitudes frequently linked to frontal systems, ridges, jet streams, lee waves, or convection (Gayet et al. 2012a; Krämer et al. 2009; Lawson et al. 2006; Muhlbauer et al. 2014; Stith et al. 2014; Jackson et al. 2015; Heymsfield et al. 2017). Ascent of humid air near midlatitude fronts, that is, in WCBs (Browning 1990), rapidly transports water into the upper troposphere. As the rising air cools, water droplets may form, and some of the droplets may freeze heterogeneously below 0°C. The ice particles can be uplifted in the front, get detrained from the system's core, and survive in its outflow for long times (Spichtinger et al. 2005). At higher altitudes, ice may also nucleate directly in situ without a liquid cloud origin. As atmospheric conditions higher up are different and less water vapor is available for condensation, the in situ–formed cirrus particles may have different properties than the uplifted liquid-origin cirrus, which is one of the hypotheses to be tested with the ML-CIRRUS experiment.

In situ ice formation takes place via homogeneous nucleation of aqueous aerosol (Kärcher and Lohmann 2002) or by heterogeneous nucleation (DeMott et al. 2003; Spichtinger and Gierens 2009b) aided by the presence of a foreign substance (Vali et al. 2015). It has been suggested that homogeneous freezing is the dominant pathway for cirrus cloud formation (Kärcher and Strom 2003). Yet, heterogeneous ice nuclei were found in a major subset of cirrus samples (Cziczo et al. 2013), calling into question the relative roles of the different ice nucleation mechanisms. This leads to a suite of questions to be addressed by the ML-CIRRUS experiment: What is the role of homogeneous versus heterogeneous nucleation for midlatitude cirrus? What are the chemical and microphysical properties of the ice residuals? How large is the occurrence frequency of in situ and liquid-origin cirrus in midlatitudes? Do they have different properties? What is the climatic importance of selected midlatitude cirrus regimes?

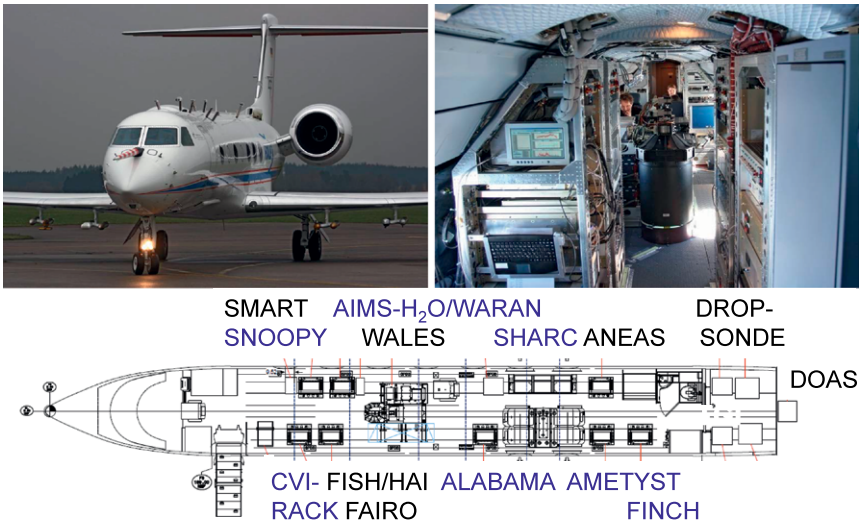

Fig. 2. HALO with comprehensive cabin instrumentation (novel instruments marked in blue), including a lidar system for the remote sensing of clouds and water vapor and an extensive in situ payload to measure ice water content, ice residuals, aerosol, trace gases, and radiation. Details of the instruments are given in Table 2.

Table 2. HALO cabin instrumentation for ML-CIRRUS. The cabin instrumentation includes instruments to measure cloud properties, aerosol, water vapor and other trace gases, and radiation. It combines in situ and remote sensing instruments including a differential absorption lidar instrument.

Instrument	Measured properties and range	Principal investigator (Institution)
WALES high-spectral-resolution lidar with H_2O differential absorption channel	H_2O profile, aerosol/cirrus extinction, depolarization, lidar/color ratio	Wirth (DLR)
Albedometer for Spectral Modular Airborne Radiation Measurement System (SMART)	Spectral radiance, spectral irradiance I = 350–2,200 nm	Wendisch (Uni Leipzig)
Counterflow Virtual Impactor inlet with CPC/UHSAS/particle and soot absorption photometer (PSAP) (HALO–CVI)	Cloud residual number concentration, absorption coefficient, size distribution 65 nm–1 μm	Mertes (TROPOS)
Aerosol Measurement System with condensation particle counters (CPCs)/optical particle counters (OPCs)/differential mobility particle sizer (DMPS)/PSAP (AMETYST)	Size distribution of total and nonvolatile aerosol, 4 nm–2 μm, absorption	Minikin/Weinzierl (DLR)
Aircraft-based Laser Ablation Aerosol Mass Spectrometer (ALABAMA)	Chemical composition of aerosol/cloud residuals > 150 nm	Schneider/Borrmann (MPI-C/Uni Mainz)
Fast Ice Nuclei Chamber (FINCH)	Total and biological ice nuclei concentrations	Rose/Curtius (Uni Frankfurt)
Single Particle Soot Photometer SP2 (SNOOPY)	Refractory black carbon mass and number concentration (85–510 nm d_equiv)	Weinzierl (DLR)
Lyman a Fluorescence Hygrometer (FISH)	H_2O, total or gas phase water, 1–1,000 ppm	Krämer (FZJ)
Hygrometer for Atmospheric Investigation Tunable Diode Laser (HAI)	H_2O, total and gas phase water, 1–40,000 ppm	Ebert/Krämer (PTB/FZJ)
Sophisticated Hygrometer for Atmospheric Research Tunable Diode Laser (SHARC)	H_2O, gas phase water, 20–40,000 ppm	Zöger (DLR)
Airborne H2O Mass Spectrometer (AIMS–H2O)	H_2O, gas phase water, 1–500 ppm	Voigt/Kaufmann (DLR)
Water Vapor Analyzer, Tunable Diode Laser Hygrometer (WARAN)	H_2O, total or gas phase water, 50(1)–40,000 ppm	Voigt (DLR)
Fast Airborne Ozone monitor (FAIRO)	O_3	Zahn (KIT)
Atmospheric Nitrogen oxides Measuring System chemiluminescence detector (AENEAS)	NO, NO_y, aircraft tracer, 5 ppt–60 ppb	Ziereis (DLR)
Dropsondes	Temperature profile, humidity	Kaufmann (DLR)
Differential Optical Absorption Spectrometer (DOAS)	NO_2, O_3, SO_2, HCHO, BrO, OClO	Pfeilsticker (Uni Heidelberg)
Basic HALO Measurement and Sensor System (BAHAMAS)	T, u, v, meteorological and aircraft state parameters	Giez (DLR)

Natural cirrus clouds can be modified by aviation. The resulting contrail cirrus contribute ~50 mW m^{-2} to global warming (Burkhardt and Kärcher 2011; Schumann and Graf 2013), with far larger regional contributions. Hence, the radiative forcing from contrail cirrus is larger than the temporally integrated radiative effects from aircraft CO_2 emissions.

A contrail is not a homogeneous object (Schumann et al. 2017) and has varying properties from local to global scales caused by complex vortex dynamics, wind shear, and mixing with ambient air (Heymsfield et al. 2010; Jeßberger et al. 2013; Petzold et al. 1997; Schröder et al. 2000; Voigt et al. 2010). Little information exists on the ice particle habit and surface structure (Gayet et al. 2012b; Schumann et al. 2011). Initially, line-shaped contrails (Voigt et al. 2011) develop into contrail cirrus and their further evolution can be detected from satellites (Iwabuchi et al. 2012; Minnis et al. 2013; Vazquez-Navarro et al. 2015). Contrail cirrus clouds are difficult to discriminate from natural cirrus in

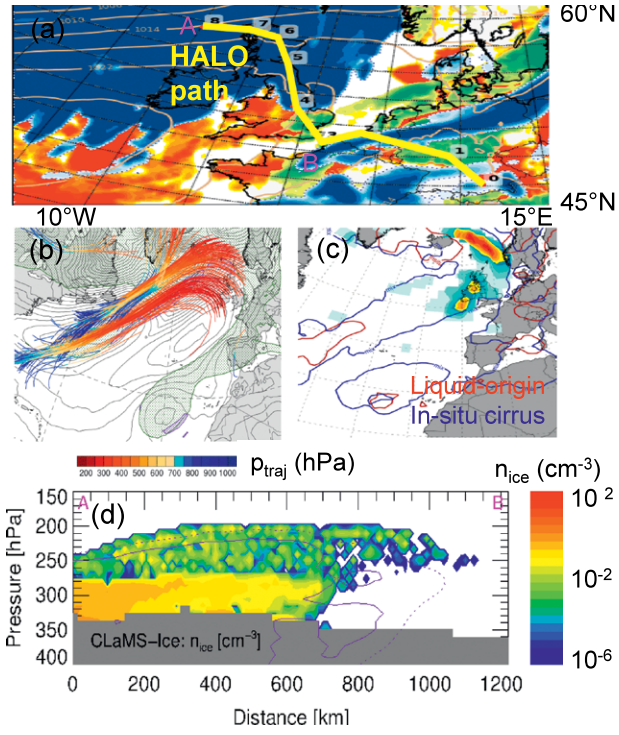

Fig. 3. The ML-CIRRUS campaign was supported by advanced cirrus forecast products: (a) ECMWF forecasts of meteorological parameters, high (blue), medium (green), and low (red) cloud cover at 1200 UTC 11 Apr 2014, and HALO flight path (yellow) into a warm conveyor belt; (b) WCB trajectories calculated from high-resolution ECMWF forecasts colored with pressure; (c) probability of occurrence of WCB trajectories (colors) and areas with predicted in situ cirrus (blue) and lifted liquid-origin cirrus (red), calculated from the ECMWF ensemble prediction system; and (d) vertical profile of CLAMS ice cirrus forecast of the ice number density along the planned flight track from A to B in (a) on 11 Apr 2014.

remote sensing analysis unless correlations with air traffic or other information can be used. Therefore, a combination of in situ and remote sensing methods including a lidar may be the most promising to investigate ice crystal microphysics in contrail cirrus. Hence, ML-CIRRUS addresses the following challenging questions related to aviation: What are the microphysical and radiative properties of contrail cirrus? Can we distinguish contrail cirrus from natural cirrus? Are contrail cirrus predictable? Can uncertainties in the climate impact from contrail cirrus be reduced using data from the ML-CIRRUS experiment?

HALO INSTRUMENTATION. To obtain a broad dataset on properties of natural cirrus and contrail cirrus for process studies and climatological analysis, we equipped HALO with state-of-the-art instrumentation, including a suite of novel cloud probes, a lidar system for remote sensing of cloud optical properties and water vapor, and a comprehensive, in situ cabin instrumentation to measure ice residuals, aerosol, trace gases, and radiation. Thereby, ML-CIRRUS was the first HALO mission with in situ cloud instrumentation (Fig. 1), followed by a mission focusing on convection in the Amazon basin in summer 2014 (Wendisch et al. 2016). The instruments were selected to cover the expected range of cloud properties and ambient conditions.

In particular, HALO is equipped with a basic sensor and data system that measures a variety of important meteorological and aircraft state parameters. Instrumental details and their acronyms are given in Tables 1 and 2. The advanced cloud instrumentation (Fig. 1) included, from large to small particle sizes, two precipitation and ice particle imagers (Weigel et al. 2016), two cloud combination probes (Weigel et al. 2016), and two light-scattering spectrometers (Schnaiter et al. 2016). The particle probes were equipped with antishattering tips, where appropriate. Further, two aerosol spectrometers (Minikin et al. 2003) and a microwave temperature profiler were mounted in wing stations. Thus, information on the complete particle size distribution from 0.5 μm to 6.4 mm, and on particle phase, shape, roughness, and complexity as well as scattering phase function and extinction, can be derived from the cloud probes and compared to remote sensing and bulk ice information from the comprehensive cabin instrumentation.

The HALO payload (Fig. 2) further included a high-spectral-resolution light detection and ranging (lidar) instrument (Wirth et al. 2009; Groß et al. 2014) to derive vertical profiles of humidity and cloud/aerosol extinction. Spectral irradiances and radiances in the solar range were observed by an albedometer (Ehrlich et al. 2008; Wendisch et al. 2007). In addition, total water (gas phase plus particulate water) or water vapor were measured in situ with a set of five hygrometers including a Lyman-α fluorescence instrument (Meyer et al. 2015; Zöger et al. 1999), an airborne water vapor mass spectrometer (Kaufmann et al. 2014, 2016), and tunable diode laser instruments with four channels based on first principles (Buchholz et al. 2014, 2017), two channels, or one channel (Voigt et al. 2014). A counterflow virtual impactor and a submicrometer aerosol inlet have been newly designed for HALO, and the aerosol instruments were switched between the inlets. Aerosol composition was measured with a single-particle laser ablation mass spectrometer (Brands et al. 2011), and refractory black carbon was measured with a single-particle soot photometer (Dahlkötter et al. 2014) and a particle soot absorption photometer. Further, the capability of aerosol to be activated to an ice particle

was detected (Bundke et al. 2008). The number concentration and size distribution of the ice residuals, that is, aerosol particles that remain after sublimation of the ice in the counterflow virtual impactor inlet, were measured using a condensation particle counter and a high-sensitivity aerosol spectrometer. In addition, the aerosol size distribution was measured with a suite of condensation and optical particle counters. Finally, the following trace gases were measured: reactive nitrogen species as aircraft tracer (Ziereis et al. 2000), ozone as tracer for photochemical production and stratospheric air (Zahn et al. 2012), as well as other tropospheric and stratospheric tracers (Prados-Roman et al. 2011; Weidner et al. 2005).

FORECAST PRODUCTS FOR ML-CIRRUS. The development of cirrus cloud forecast products based upon operational forecasts from the European Centre for Medium-Range Weather Forecasts (ECMWF) was essential to direct the aircraft into selected cirrus cloud systems. Figure 3 shows a collage of forecast products for a flight into a strong WCB over the North Atlantic on 11 April 2014. Vertical composites of meteorological data along the projected flight path were calculated with the meteorological mission support tool (Rautenhaus et al. 2012). The occurrence of warm conveyor belts (Schäfler et al. 2014) with an ascent of more than 600 hPa in 48 h were calculated by ETH Zürich (Sprenger and Wernli 2015), using ECMWF deterministic and ensemble forecasts. After the campaign, 10-day backward trajectories were calculated from the HALO flight paths with the same trajectory tool, and the updraft velocity, ice water content (IWC), and liquid water content (LWC) along the trajectories were evaluated to get insight into ice formation processes. In addition, a cirrus model (Spichtinger and Gierens 2009a) was coupled to the global Chemical Lagrangian Model of the Stratosphere (CLAMS; Grooss et al. 2005) in order to predict microphysical cirrus properties such as size and number density (Luebke et al. 2016). Further, the Contrail and Cirrus Prediction model (CoCiP; Schumann 2012; Schumann and Graf 2013) was developed for accurate contrail cirrus predictions. CoCiP is a Lagrangian model that traces individual contrails forming behind aircraft flying along given flight routes for given ambient meteorology. Hourly predictions of cirrus and contrail optical depth were used to decide on the target area and timing of the individual flights.

Table 3. Overview of the ML-CIRRUS flights. Date, mission scope, target region, meteorological information, and flight durations are given. Multiple flights in the same day are labled "a" and "b" in the date column.

Mission No.	Date	Mission scope	Target region	Additional observations/remarks	Flight duration
1–3	21–22 Mar a, b	Three instrument test flights	Germany	—	6 h
4	26 Mar 2014	Contrails and contrail cirrus	North Atlantic flight corridor	—	8 h 30 min
5	27 Mar 2014	Frontal cirrus, WCB in- and outflow	Alps, Italy, Germany	—	4 h 45 min
6	29 Mar 2014	Lee-wave cirrus, WCB, jet stream divergence, convective cirrus	France, Spain	Lower cloud layers with Saharan dust	7 h 30 min
7	1 Apr 2014	Cirrus, contrail cirrus	Germany	Ludwig Maximilians Universität (LMU), Deutscher Wetterdienst (DWD), Leipzig lidar	6 h 35 min
8	3 Apr 2014	Frontal cirrus, WCB outflow	Germany	—	5 h 15 min
9, 10	4 Apr 2014 a, b	Clean jet stream cirrus, polluted WCB	Spain, Portugal	CALIPSO overpass, double flight	9h 55 min
11	7 Apr 2014	Contrail cirrus, cirrus sublimation, Halo	Germany	MIM, Leipzig lidar H_2O sonde	5 h 35 min
12	10 Apr 2014	Contrails and contrail cirrus	Germany	Contrail probing	3 h 15 min
13, 14	11 Apr 2014 a, b	Frontal cirrus, large WCB, ridge cirrus	Great Britain	Lagrangian approach, double flight	10 h
15	13 Apr 2014	High pressure system, jet stream cirrus	France, Spain, Portugal	Many contrails	7 h 15 min
16	15 Apr 2014	Föhn, divergence, gravity wave cirrus	Alps	Instrument tests: liquid cloud, aerosol inlet	3 h

After the campaign, a database of realistic air traffic data were set up from various sources, and CoCiP was rerun with hourly ECMWF numerical weather prediction data including assimilated observation data. Figure 4 shows maps with 2.4- and 0.4-day forecasts of the optical depth of contrail cirrus and natural cirrus, which motivated our first ML-CIRRUS science flight heading for contrail cirrus.

ML-CIRRUS FLIGHT STRATEGY, FLIGHT PATHS, AND SCOPE OF THE INDIVIDUAL FLIGHTS. The synergetic use of the different forecasts allowed for targeted flights into selected cirrus cloud regimes. Altogether during ML-CIRRUS, the HALO research aircraft performed 16 flights in midlatitude cirrus and contrail cirrus with a total of 88 flight hours. Cirrus clouds were probed for more than 40 h either with the in situ or the remote sensing instrumentation. The HALO flight tracks are shown in Fig. 5, and regions where cirrus were probed with in situ instruments indicated by the IWC derived from Water Vapor Analyzer, Tunable Diode Laser Hygrometer (WARAN)/ Sophisticated Hygrometer for Atmospheric Research Tunable Diode Laser (SHARC) hygrometers are color coded. Extensive cirrus measurements were performed above west Europe and the Atlantic from 36° to 58°N and from 15°E to 15°W. Generally, the flight strategy was selected to directly probe the cirrus with the in situ instrumentation and then perform high-altitude legs above the cirrus along the same coordinates for remote sensing of the cirrus. Quasi-Lagrangian measurements along air mass trajectories were performed to investigate the evolution of cirrus properties along the cirrus' life cycle. Collocated MSG data were evaluated to analyze the clouds' horizontal extensions and cirrus optical depths. One flight was specifically dedicated for the validation of *CALIPSO* data products. For contrail cirrus flights, air traffic control centers in Karlsruhe and Shannon were contacted 6 months before the start of the campaign in order to get support for the campaign and permission for HALO operation in and near air traffic corridors. Flight plans were submitted to air traffic control 2 days in advance and were refined 24 h prior to the flight. In addition, depending on meteorological conditions, areas with temporary restricted access for general aviation were blocked for contrail cirrus flights a day in advance. HALO independently and freely operated within these areas, directed inflight by the mission scientist onboard.

The scopes of the individual flights, the measurement region, and the meteorological situation for each flight are presented in Table 3. The ML-CIRRUS airborne experiment focused four flights on the detection of cirrus in strong frontal and ridge systems and in particular probing the outflow region of WCBs. Further, jet stream–induced as well as synoptic cirrus linked to high pressure systems were probed over the Atlantic Ocean, the Mediterranean Sea, and western Europe, orographically induced mountain wave cirrus were measured over the Pyrenees, and a convective system was probed over the Mediterranean Sea. Less-polluted cirrus were measured over the Atlantic, while cirrus above the European continent could have encountered significant anthropogenic pollution. For more than a week in early April 2014, a strong Saharan dust outbreak produced headlines in European news media. The Saharan dust was transported to Europe and impacted some of the flights. Although the main dust layers were located in the middle and lower troposphere, a small fraction of the desert dust particles may have reached cirrus altitudes. A first analysis shows that the quality of the forecast from ECMWF in terms of cloud cover is significantly reduced in the presence of mineral dust.

HIGHLIGHTED RESULTS FROM ML-CIRRUS. The analysis of ML-CIRRUS data addresses the topics of intense cirrus research introduced before, and selected results are briefly presented below.

Overview of midlatitude cirrus properties. During ML-CIRRUS, cirrus clouds were observed in meteorological regimes typical for European midlatitudes with a focus on frontal cirrus including WCBs. The cirrus clouds were generally observed at altitudes between 7 and 13.5 km and at temperatures above 203 K. IWC in midlatitude cirrus derived from Hygrometer for Atmospheric Investigation Tunable Diode Laser (HAI)/ SHARC hygrometers ranged between 10^{-6} and 0.2 g m^{-3} and was highly variable (Fig. 6a). As expected from previous studies, for example, Wang and Sassen (2002) or Schiller et al. (2008), the median IWC shows a dependence on temperature because more water vapor is available for condensation and growth of ice particles at higher temperatures. Future work will compare the IWCs derived from in situ cloud probes and bulk instruments in more detail. Ice number densities derived from the Novel Ice Experiment—Cloud and Aerosol Particle Spectrometer (NIXE–CAPS) instrument (Fig. 6b) ranged between 10^{-4} and ~20 cm^{-3} and were often between 0.05 and 0.5 cm^{-3}. High particle number densities (>5 cm^{-3}) were observed in contrails over Germany and the Atlantic. Hence, contrail cirrus clouds were frequently encountered during ML-CIRRUS and cirrus clouds are often influenced by air traffic in European midlatitudes.

The in-cloud relative humidity with respect to ice (RHi) is centered near 100% (Fig. 6c) over the complete cirrus temperature range, as derived from airborne mass spectrometer AIMS–H_2O data (Kaufmann et al. 2016), consistent with previous observations (Krämer et al. 2009; Ovarlez et al. 2002). The range of RHi in cirrus is bounded on the upper side by the homogeneous nucleation threshold temperatures (Koop et al. 2000). Low RHi values are measured occasionally in cirrus, indicating that cirrus clouds exist also in strongly ice-subsaturated air masses. Nonequilibrium conditions, for example, caused by particle sedimentation or fast warming of descending air explain these low values.

Cirrus origin. To categorize cirrus with respect to their formation history, 10-day back trajectories starting on the HALO flight path every 10 s were calculated with the Lagrangian analysis tool (LAGRANTO) and the IWC and LWC along the backward trajectory where the observed cirrus segment were derived (Wernli et al. 2016). This approach distinguishes whether the air parcel has been in a mixed-phase cloud before with both LWC > 0 and IWC > 0 and classifies it as liquid-origin cirrus. Otherwise, cirrus clouds with an air parcel trajectory with IWC only and without LWC are defined in situ cirrus. As an example for liquid-origin cirrus, we show here results from the flight into the outflow region of a large WCB above Great Britain (see also Fig. 3) on

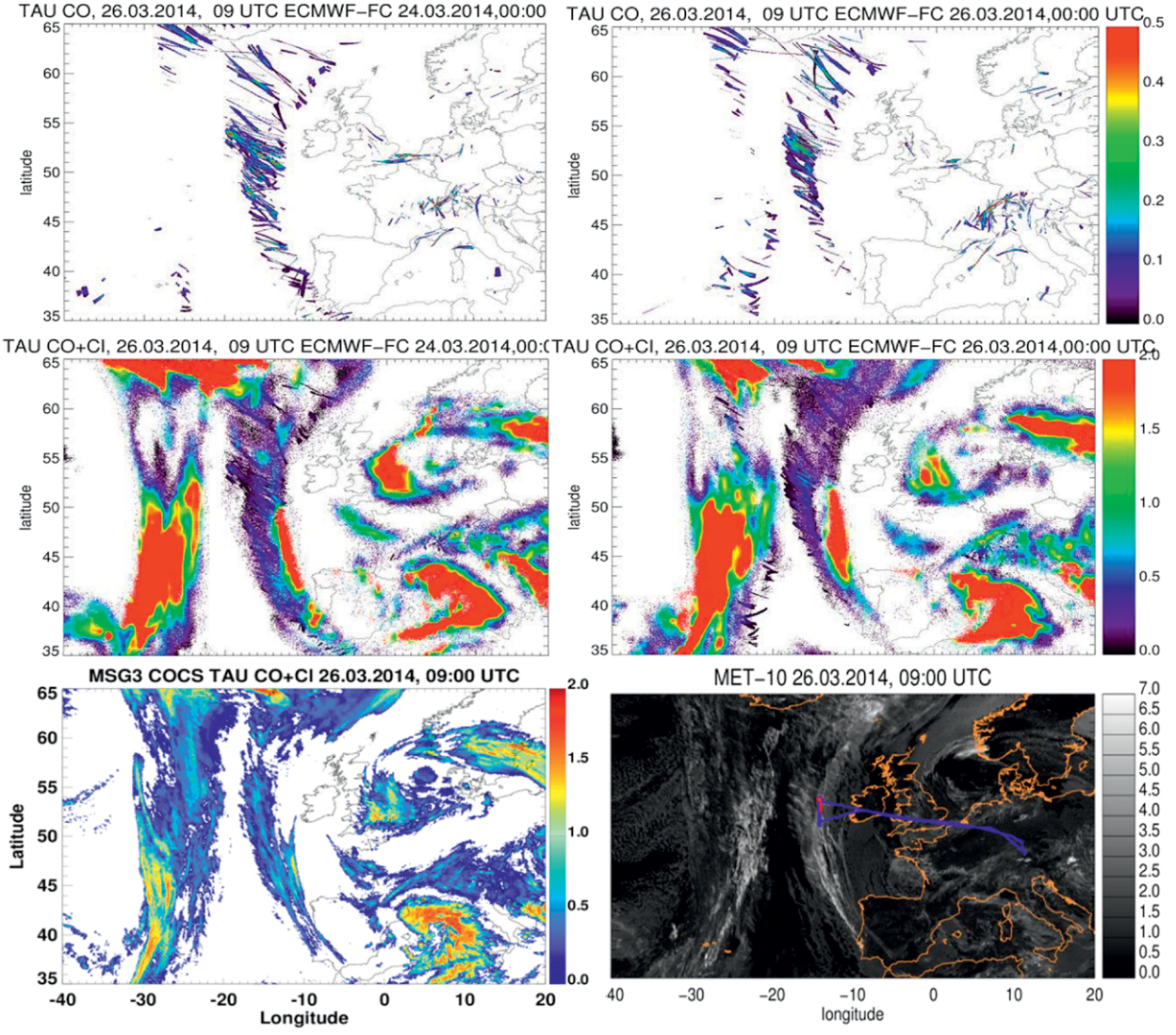

Fig. 4. Maps with 2.4- and 0.4-day forecasts of optical depth at 550 nm of (top) contrails and (middle) contrail cirrus and cirrus at 0900 UTC 26 Mar 2014 calculated with CoCiP. (bottom left) Cirrus optical depth derived from Meteosat Second Generation–SEVIRI at 0900 UTC 26 Mar 2014; (bottom right) brightness temperatures difference from 10.8 to 12 μm from MSG with the HALO track (blue line) and the position of HALO (red) at the time of the MSG analysis. The comparison confirms the good quality of the CoCiP contrail and cirrus predictions.

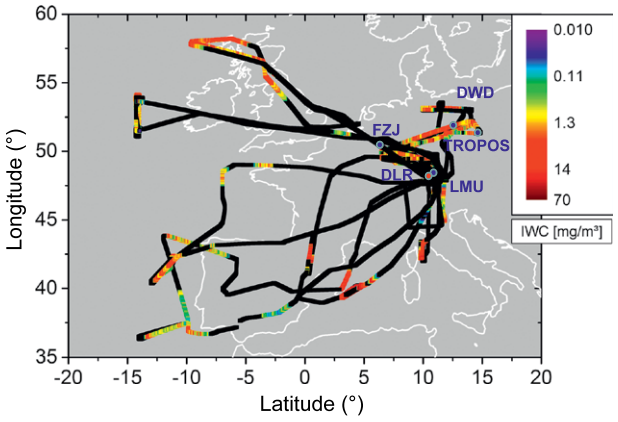

Fig. 5. Flight paths of HALO during the ML-CIRRUS experiment. HALO performed 16 flights above Europe and the Atlantic. The ice water content along the flight track derived from WARAN/SHARC hygrometers is color coded. The locations of the ground-based stations integrated into the HALO flight planning are given by the blue circles; the red circle denotes the aircraft base at DLR Oberpfaffenhofen.

11 April 2014. Figure 7 shows profiles of lidar backscatter ratios at 532 nm along the Lagrangian flight track and the altitude of the in situ flight leg. A 3-km-thick cirrus layer extended up to 12-km altitude. The ice particle size distribution derived from cloud and aerosol spectrometer with depolarization (CAS–DPOL), cloud imaging probe (CIP), and precipitation imaging Probe (PIP) at 9.8-km altitude and at 1440 UTC is given in Fig. 7b. According to the trajectory approach described above, (see also Wernli et al. 2016) the analyzed cloud segment is classified as liquid-origin cirrus. Thus, ice particles originating from a mixed-phase cloud lifted to higher altitudes may contribute to the particle size distribution. In addition, the particle size distribution of a cirrus cloud segment measured at 1521 UTC classified as in situ cirrus is given in Fig. 7c. Smaller mean particle diameters and smaller IWC were measured in the in situ cirrus compared to the liquid-origin cirrus in this case, detected at the same altitude and temperature (228 K) near 100% RHi.

Liquid-origin and in situ cirrus were introduced recently by Krämer et al. (2016) by comparison of model simulations and field observations. They analyzed cirrus properties in different geographical regions from an extensive dataset and found higher IWCs and larger ice crystals in liquid-origin compared to in situ cirrus. Luebke et al. (2016) investigated the two cirrus types in more detail based on ML-CIRRUS observations by using a trajectory-based approach similar to this study. Their analysis confirmed the results by Krämer et al. (2016), but, in addition, higher crystal concentrations were found in liquid-origin cirrus.

We further investigate the occurrence frequency of in situ and liquid-origin cirrus along all ML-CIRRUS flight paths (Fig. 8). In line with the study of Luebke et al. (2016), for the observation region in European midlatitudes and the encountered atmospheric conditions, a high abundance of in situ cirrus is found at temperatures below −55°C. At warmer temperatures (from −35° to −50°C), both types, in situ and liquid-origin cirrus, were measured. This can vary for other latitudes or seasons, where different dynamic situations prevail. Generally, regarding the synoptic situation, liquid-origin cirrus clouds are often linked to frontal systems, WCB, or ridge cirrus and can be found in convection. In situ cirrus clouds are typically linked to jet streams, synoptic high pressure systems, or mountain waves.

Ice particle complexity. For similar reasons, different ice particles' complexities are expected in the selected cirrus types, as discussed below. Thereby, the small-scale ice particle complexity refers to any kind of ice crystal perturbations (surface roughness on different scales, inclusions, polycrystalline habits, and hollowness) that result in a diffuse spatial distribution of the scattered light (Schnaiter et al. 2016). Small-scale complexity is used here to differentiate the single particle complexity to the large-scale complexity induced by crystal aggregation. It describes surface defects on the submicrometer to micrometer scale that can be detected by measurements of the spatial uniformity of coherent light scattering. The small-scale complexity parameter k_e derived from Small Ice Detector Mark 3 (SID-3) measurements shows a robust correlation with the degree of physical surface defects in the above scale range (Schnaiter et al. 2016). The threshold value for k_e of 4.6 defines the transition from a nearly undisturbed (left inlay) to a more uniform (right inlay) spatial light scattering behavior of pristine and complex ice crystals, respectively. The distribution of k_e in in situ cirrus probed on 4 April 2014 is presented in Fig. 9. The jet stream cirrus had formed in unpolluted conditions at the coast of Portugal. Roughly 80% of the probed particles showed a crystal complexity above the k_e threshold, indicating that the crystals nucleated and grew at elevated humidity conditions that promote crystal surface defects. Homogeneous nucleation in aqueous aerosol particles at high supersaturations is a plausible formation pathway that explains the high ice particle complexity observed in this case.

Synergy between aircraft and ground-based measurements was achieved by coordinated HALO overpasses of the rooftop remote sensing instrumentation at the Ludwig Maximilian University of Munich, which aimed for observations of ice particle shape and

orientation using information of halo displays. On 1 April 2014, three overpasses were performed when a large and relatively homogeneous cirrus layer was present. Different halo displays were detected between 0800 and 1300 UTC on that day: 22° halo, upper tangent arc, circumscribed halo, Parry arc, and sundogs. The comparison of ground-based ice crystal shape observations with data from the airborne cloud probes indicates that even though halo displays were visible, the majority of ice crystals in the cirrus cloud were rough or complex.

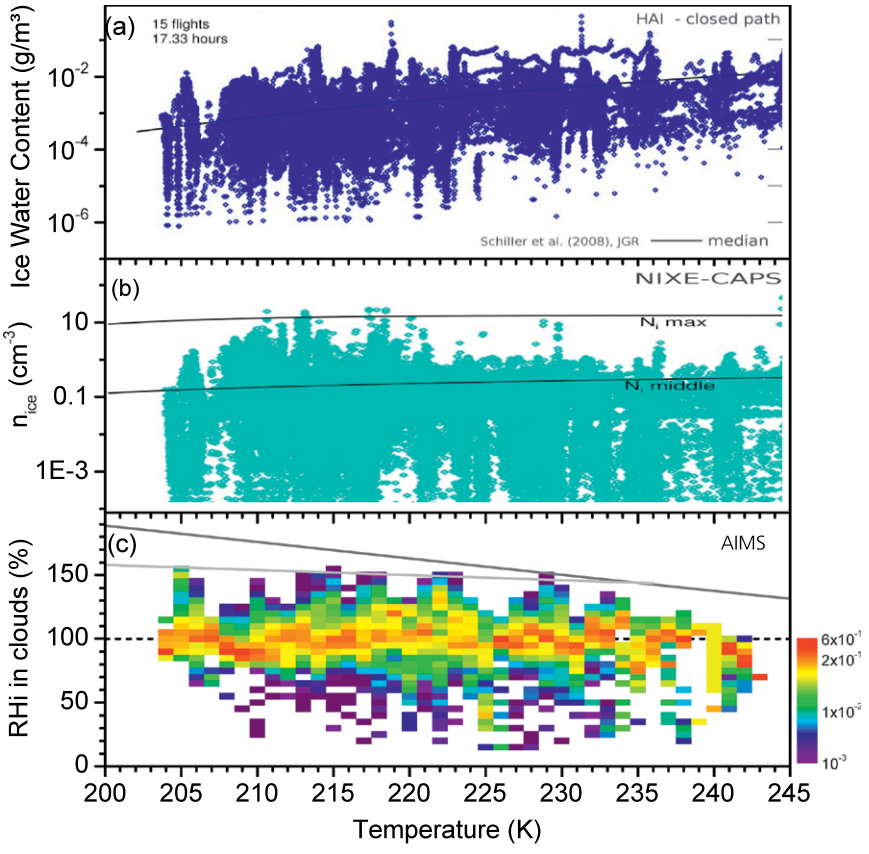

Fig. 6. (a) Range and temperature dependence of the IWC detected during ML-CIRRUS derived from HAI/SHARC hygrometers (blue dots) and median from Schiller et al. (2008) (black line). (b) Ice number densities in the size range of 3- to 937-μm diameter (N_i) in cirrus from NIXE–CAPS and middle and maximum N_i from Krämer et al. (2009). (c) Relative frequency of RHi in cirrus from AIMS–H2O (Kaufmann et al. 2016) and Basic Halo Measurement and Sensor System (BAHAMAS) temperature data in 1-K temperature bins. The light gray line shows the homogeneous nucleation threshold from Koop et al. (2000) and the dark gray line shows the liquid water saturation (Murphy and Koop 2005).

Ice residuals and aerosol. The composition and size of ice residuals were detected with the Aerosol Laser Ablation Mass Spectrometer (ALABAMA; Brands et al. 2011) and an Ultra-High Sensitivity Aerosol Spectrometer Airborne (UHSAS) connected to the HALO–Counterflow Virtual Impactor (CVI) inlet. Figure 10 shows results from a cirrus flight above Germany with many contrail cirrus on 7 April 2014. The measured residuals with sizes larger than 150 nm are classified according to their composition, and the relative numbers of particles with a specific composition are given in the pie chart. The major number contribution to the ice residuals and to the upper-tropospheric background aerosol at 8–10-km altitudes comes from potassium and its mixtures with sulfate, nitrate, and organics. Potassium is an indicator for a biogenic aerosol source (both biomass burning and primary biological aerosol). In addition, about 10% by number of ice residuals are composed of black carbon, which is less than the black carbon fraction in the background aerosol. Young aviation soot generally has sizes smaller than 150 nm and therefore cannot be detected with this instrumentation. Thus, the measured black carbon–containing particles could be either aged aviation soot particles that had time to grow by condensation and/or coagulation or they could have a boundary layer origin, for example, fossil fuel or biomass burning. In addition, lower-stratospheric aerosol spectra (not shown here) contain a significant contribution from meteoric material. Compared to ambient upper-tropospheric aerosol, the ice residuals contain a smaller fraction of black carbon but a slightly higher fraction of particles containing minerals and metals (Fig. 10). However, the general similarity between ice residues and the upper-tropospheric aerosol suggest that homogeneous freezing seems to dominate cirrus cloud formation in this case. Heterogeneous freezing would lead to an enhancement of specific, ice nucleating particles in the ice residues. This is not the case here, at least not to a significant extent. Generally during ML-CIRRUS, sulfur is found in many of the ice residuals, often in combination with other compounds. One may therefore speculate on the importance of

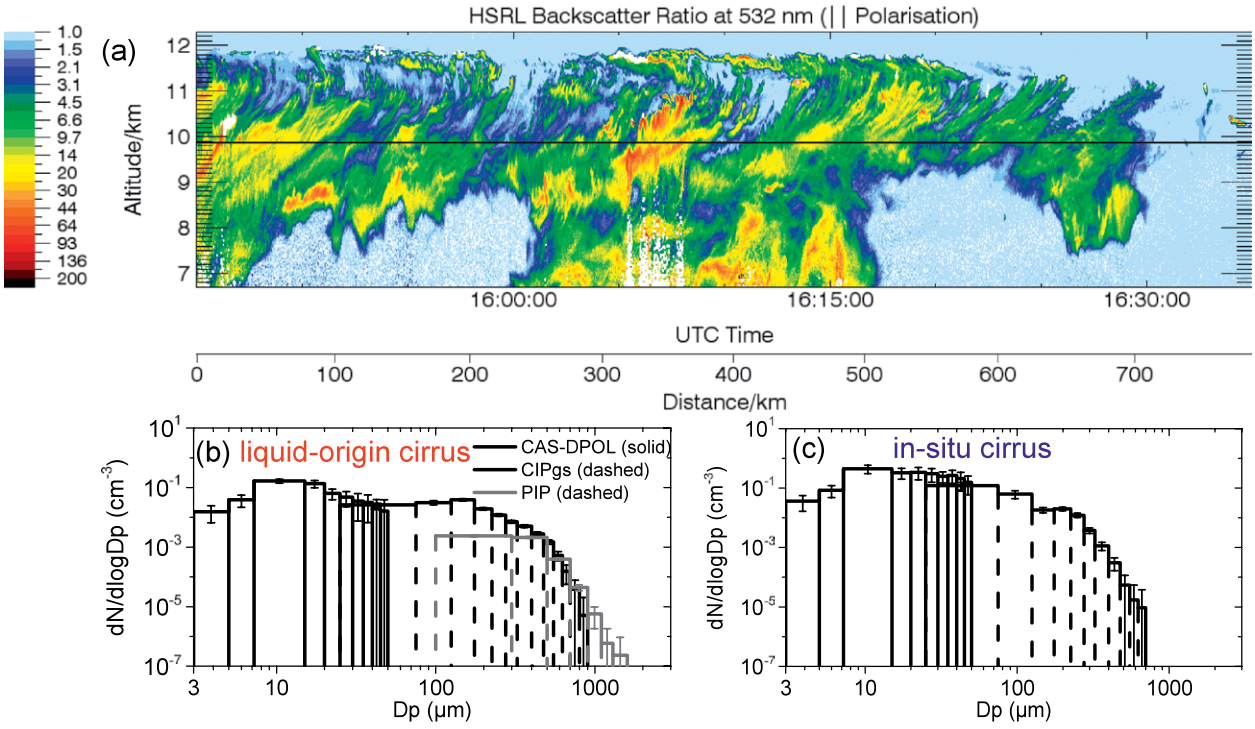

Fig. 7. (a) Quasi-Lagrangian measurements in a WCB cirrus above England on 11 Apr 2014. Backscatter ratios at 532 nm derived from the WALES lidar along a quasi-Lagrangian flight segment shown in Fig. 3 from A to B. The flight altitude at 9.8 km of the preceding in situ flight leg is given by the black line. (b) The particle size distribution in a liquid-origin cirrus classified by trajectory analysis detected at 1440 UTC and 9.8-km altitude derived from CAS–DPOL, CIP, and PIP data; (c) particle size distribution for an in situ cirrus detected at 1521 UTC.

homogeneous nucleation for cirrus formation, even though the existence of sulfate can originate from heterogeneous drop freezing processes as well. A bimodal particle size distribution of the ice residuals has been detected on the same day (Fig. 11). The presence of a small mode with particles sizes below 70 nm, possibly aircraft emissions, and a second mode centered near 160 nm suggests different ice residual compositions or origins. The aerosol composition detected by the aerosol mass spectrometer (Fig. 10) refers to the second mode only because the smallest particle size that can be detected by ALABAMA is about 150 nm. A detailed investigation of the ice crystal number in the different cirrus types and in contrail cirrus versus the ice residual number is planned.

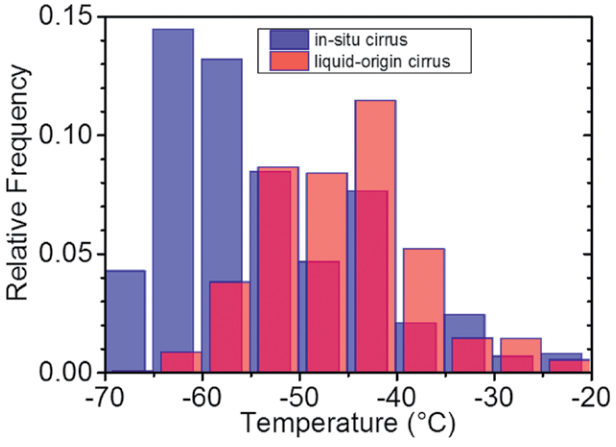

Fig. 8. Analysis of the origin of midlatitude cirrus: the relative frequency of occurrence of cirrus along the ML-CIRRUS flight tracks with a liquid-origin (red; LWC along the ECMWF trajectory > 0.01 mg kg^{-1}) and an in situ origin (blue; only IWC along trajectory) are shown. In situ cirrus clouds dominate the distribution at T < −55°C and both types occur at higher T.

Validation of satellite products. Several satellite data products were validated using ML-CIRRUS measurements. A MODIS overpass on 13 April 2014 matching the flight pattern of HALO was used to compare the spectral nadir radiance measured by Spectral Modular Airborne Radiation Measurement System (SMART) and MODIS in a cirrus situation west of the Iberian Peninsula. Figure 12 shows spectral nadir radiances averaged for a cirrus overflight between 1347 and 1403 UTC. The full spectrum measured by SMART and band-average radiances of SMART and MODIS are shown. Except for the 1.24-μm band, differences range within the instruments' uncertainties (5% for

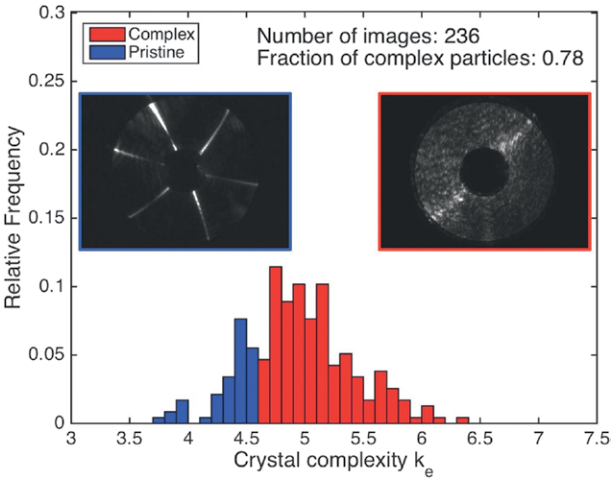

Fig. 9. Ice crystal complexity k_e measured with SID-3 of an in situ origin cirrus at the coast of Portugal on 4 Apr 2014. About 80% of the probed particles show k_e above a threshold value of 4.6, indicating a high surface roughness.

all MODIS bands; 2% below and 5% above 1 μm for SMART). This agreement is excellent and indicates a consistent radiometric calibration of both instruments. The SMART observations will further be used for validation of the MODIS cirrus retrieval products.

Predictability of contrail cirrus. The goals of the CoCiP (Schumann et al. 2012) were threefold: to predict contrail cirrus and to guide the HALO aircraft into selected contrail cirrus situations, to validate the model with ML-CIRRUS data in order to assess contrail cirrus predictability, and to interpret contrail cirrus observations with the goal to better understand today's contrail cirrus radiative forcing uncertainties. On 23 March 2014, CoCiP predictions suggested good observation conditions for contrail cirrus near the eastern end of the oceanic flight corridor for 26 March 2014 (see Fig. 4). The weather at that time was controlled by a WCB outflow causing an elongated cirrus band near the coast of Great Britain. Many long-lived contrails were expected from the traffic in the North Atlantic flight corridor. We chose the late morning period (0800–1200 UTC) for a flight because the low traffic density at this time allowed for measurements in the air traffic corridor under Shannon radar control. The aged contrails were generated during the early morning hours and drifted with the mean wind into the target area at 10°–14°W. The final predictions prior to takeoff on 26 March 2014 confirmed the predictions obtained 3 days earlier; hence, we decided to take off for the first scientific mission flight. During the flight, the mission scientist reported that HALO was indeed measuring in and above cirrus and young and aged contrails. Figure 4 includes two contrail cirrus forecasts and SEVIRI satellite data at the time of flight. White areas in the 10.8–12-μm brightness temperature difference are sensitive to thin cirrus and contrail cirrus containing many small ice particles. Indeed, the analysis shows line patterns and local maxima in the brightness temperature difference values, indicating the presence of aged contrail cirrus. The comparison of CoCiP optical thickness for natural cirrus plus contrails (Fig. 4) against the cirrus optical thickness derived from SEVIRI using an algorithm by Kox et al. (2014) confirms the good prediction of the position, extension, and the optical thickness range of the contrail cirrus band between 20° and 10°W (i.e., between –20° and –10°). In fact, the experiences made during ML-CIRRUS proved that CoCiP is a reliable source for mission planning. More detailed comparison showed that local differences between forecast and measured data exist, in particular for atmospheric humidity.

Microphysical properties of contrail cirrus. The distinction between contrails and contrail cirrus from satellite observations alone is difficult, and model results or direct observations are required. Therefore, we used simultaneous observations of the aircraft tracer

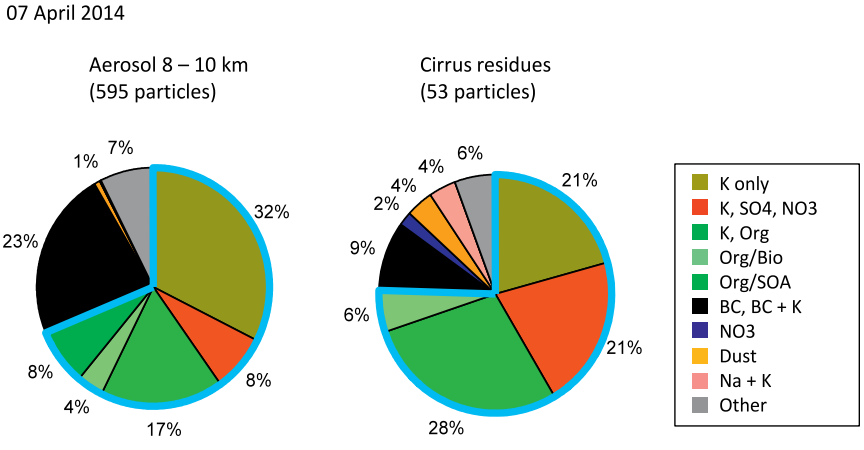

Fig. 10. Composition of the upper-tropospheric aerosol and of cirrus residuals inferred from in situ single-particle mass spectrometry. The blue-framed particle types represent the mixed upper-tropospheric background aerosol, consisting of sulfate, nitrate, organics, and potassium, which are found in similar abundance both in the cirrus residues and in the aerosol.

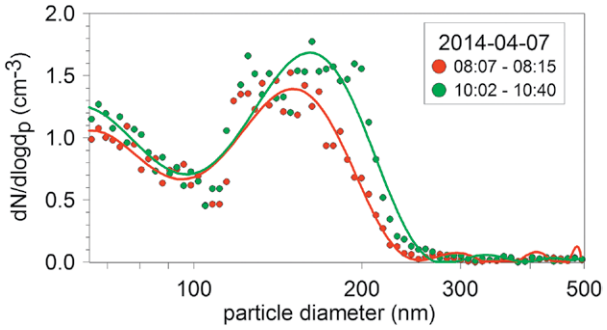

Fig. 11. Two particle size distributions of ice residuals in cirrus and contrail cirrus above Germany detected with the UHSAS connected to the HALO-CVI on 7 Apr 2014. The two modes suggest different ice residual origins.

reactive nitrogen and particle number densities to separate air masses influenced by air traffic. Then we calculated the age of the contrails from the reactive nitrogen measurements using tracer dilution correlations (Schumann et al. 1998) and CoCiP. Indeed, we frequently encountered contrails and contrail cirrus with ages up to 5 h during the contrail cirrus flight on 26 March 2014. Figure 13 shows the particle size distribution for ~3-h-old contrail cirrus observed at 1002 UTC 26 March 2014. The number densities of small ice particles (with diameters $d < 30\ \mu$m) are still enhanced compared to the surrounding cirrus, which grew under similar atmospheric conditions. Initially high particle number densities in young contrails decrease to lower values by dilution. In addition, the contrail ice crystals grow slowly by water uptake in entrained air. The microphysical properties of the probed, aged contrail cirrus still differ from natural cirrus, confirming that a signature of high particle number densities remains throughout the contrail cirrus life cycle, as suggested by model studies (Lewellen 2014; Schumann et al. 2015). The smaller particle sizes result in higher extinctions and optical depths of contrail cirrus compared to natural cirrus as indicated from satellite observations (Iwabuchi et al. 2012).

CONCLUSIONS AND OUTLOOK. The ML-CIRRUS experiment was the first cloud mission with HALO with sophisticated in situ/remote sensing instrumentation. Its data products are available at the HALO database (https://halo-db.pa.op.dlr.de/mission/2). Please contact the corresponding author for more information. Observations from satellites and ground and advanced numerical simulations were used to predict and analyze cirrus and contrail cirrus occurrence. HALO performed 16 flights in Europe in March and April 2014 with a focus on midlatitude cirrus linked to WCBs or ridges, jet streams, lee waves, and high pressure systems, and on contrail cirrus. This paper presents first highlights from the ML-CIRRUS experiment: 1) Climatological distributions of microphysical cirrus properties are provided for climate studies. 2) We gained new insights into cirrus formation in meteorological regimes typical for midlatitudes in spring. Liquid-origin cirrus clouds, classified based on trajectory analysis, are generally related to frontal systems including WCBs (or convection) and occur at warmer temperatures and lower altitudes. In situ cirrus are linked to jet streams, mountain waves, high pressure systems, and dominate cirrus occurrence at temperatures less than –55°C and higher altitudes. In a specific case, a high fraction of complex, rough

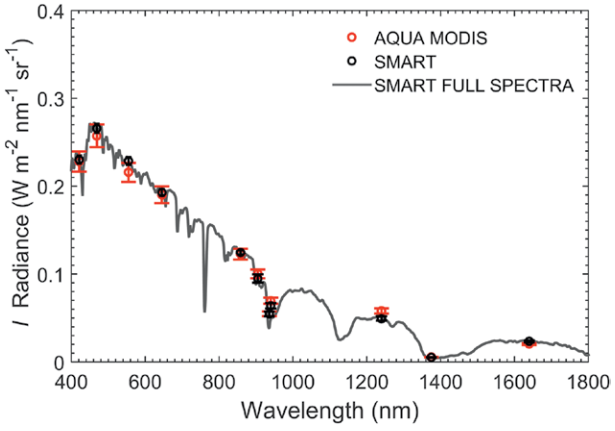

Fig. 12. Spectral radiance from SMART and MODIS averaged for a cirrus overflight during 1347–1403 UTC 13 Apr 2014 west of the Iberian Peninsula. The full SMART measurement (gray line) and band-averaged radiance of SMART (black circles) and of MODIS (red circles) data are shown. Error bars indicate the measurement uncertainty in the individual spectral bands.

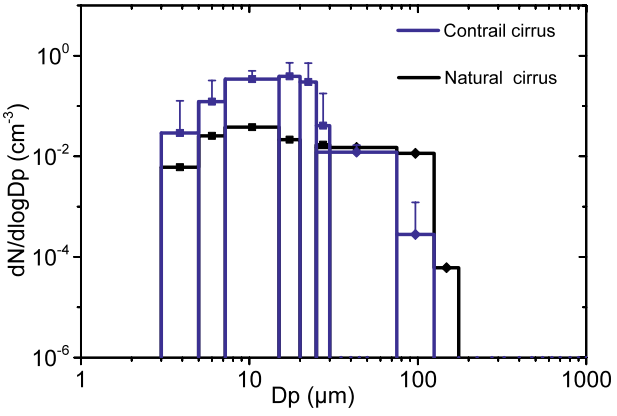

Fig. 13. Particle size distribution in a ~3-h-old contrail cirrus (blue) and the neighboring natural cirrus (black) derived from CAS-DPOL and CIP data during the contrail cirrus flight in the North Atlantic flight corridor at 1002 UTC 26 Mar 2014. Contrail cirrus clouds contain higher number densities of small ice crystals compared to natural cirrus.

ice particles is found in homogeneously nucleated in situ cirrus. For another case, the composition of the cirrus ice residuals resembles the background aerosol to a large degree, suggesting that homogeneous freezing plays a role in cirrus formation. However, slight enhancements of heterogeneous ice nuclei (mineral- and metal-containing particles) were observed in that case. 3) *Aqua*–MODIS and MSG–SEVIRI cloud data products were validated. 4) Contrails are to a large degree predictable, confirming that the basic contrail formation processes are well simulated, though further improvement potential exists. The CoCiP contrail and cirrus model is a valuable tool for applications that may enable aviation flight routing with minimal climate impact. 5) Many of the midlatitude cirrus were influenced by air traffic. Contrail cirrus clouds are clearly different from natural cirrus, which evolved under the same meteorological conditions, even at large contrail cirrus age. Altogether, ML-CIRRUS provides a comprehensive dataset on natural cirrus and aircraft-induced cloudiness in the densely populated midlatitude regions, which help to improve our understanding of cirrus and contrail cirrus and their role for climate and weather.

Future studies will concentrate on the detailed interinstrument comparison of the UTLS water vapor distribution and of microphysical and bulk ice cirrus properties in order to better constrain atmospheric conditions and to quantify instrumental uncertainties and atmospheric variability in selected parameters. A method will be derived to compare water vapor and cloud datasets with different resolutions (e.g., remote sensing and in situ). The new classification of cirrus clouds will be applied to other cirrus properties (complexity, optical depths) and climatological analysis will be performed. In the future, the processes that start or end cirrus' lifetime as well as the impact of dust events or cloud processes on the quality of weather forecasts will be evaluated in detail. The extensive contrail cirrus observations provide new information on ice particle habit, surface structure, and, in combination with models, their climate impact.

ACKNOWLEDGMENTS. We thank the DLR flight department for great support during the campaign and the pilots for excellent cooperation and flight guidance into cirrus and contrail cirrus. Support by the Helmholtz Association, the Max Planck Society, and by the German science foundation DFG within the SPP HALO 1294 is greatly appreciated. J. Schneider and R. Weigel received funding by the BMBF within the joint ROMIC-project SPITFIRE (01LG1205A). Finally, we thank M. Rautenhaus for providing the MSS tool and all the federal ministries, colleagues, partners, and funding agencies that made HALO measurements possible.

REFERENCES

Barnes, W. L., T. S. Pagano, and V. V. Salomonson, 1998: Prelaunch characteristics of the Moderate Resolution Imaging Spectroradiometer (MODIS) on EOS-AM1. *IEEE Trans. Geosci. Remote Sens.*, **36**, 1088–1100, doi:10.1109/36.700993.

Bauer, P., A. Thorpe, and G. Brunet, 2015: The quiet revolution of numerical weather prediction. *Nature*, **525**, 47–55, doi:10.1038/nature14956.

Brands, M., and Coauthors, 2011: Characterization of a newly developed Aircraft-Based Laser Ablation Aerosol Mass Spectrometer (ALABAMA) and first field deployment in urban pollution plumes over Paris during MEGAPOLI 2009. *Aerosol Sci. Technol.*, **45**, 46–64, doi:10.1080/02786826.2010.517813.

Browning, K. A., 1990: Organization of clouds and precipitation in extratropical cyclones. *Extratropical Cyclones: The Erik Palmén Memorial Volume*, C. W. Newton and E. O. Holopainen, Eds., Amer. Meteor. Soc., 129–153.

Buchholz, B., A. Afchine, and V. Ebert, 2014: Rapid, optical measurement of the atmospheric pressure on a fast research aircraft using open-path TDLAS. *Atmos. Meas. Tech.*, **7**, 3653–3666, doi:10.5194/amt-7-3653-2014.

——, A. Afchine, A. Klein, C. Schiller, M. Krämer, and V. Ebert, 2017: HAI, a new airborne, absolute, twin dual-channel, multi-phase TDLAS-hygrometer: Background, design, setup, and first flight data.*Atmos. Meas. Tech.*, **10**, 35–57, doi:10.5194/amt-10-35-2017.

Bundke, U., B. Nillius, R. Jaenicke, T. Wetter, H. Klein, and H. Bingemer, 2008: The fast ice nucleus chamber FINCH. *J. Atmos. Res.*, **90**, 180–186, doi:10.1016/j.atmosres.2008.02.008.

Burkhardt, U., and B. Kärcher, 2011: Global radiative forcing from contrail cirrus. *Nat. Climate Change*, **1**, 54–58, doi:10.1038/nclimate1068.

Chen, T., W. B. Rossow, and Y. C. Zhang, 2000: Radiative effects of cloud-type variations. *J. Climate*, **13**, 264–286, doi:10.1175/1520-0442(2000)013<0264:REOCTV>2.0.CO;2.

Cziczo, D. J., and Coauthors, 2013: Clarifying the dominant sources and mechanisms of cirrus cloud formation. *Science*, **340**, 1320–1324, doi:10.1126/science.1234145.

Dahlkötter, F., and Coauthors, 2014: The Pagami Creek smoke plume after long-range transport to the upper troposphere over Europe—Aerosol properties and black carbon mixing state. *Atmos. Chem. Phys.*, **14**, 6111–6137, doi:10.5194/acp-14-6111-2014.

DeMott, P. J., D. J. Cziczo, A. J. Prenni, D. M. Murphy, S. M. Kreidenweis, D. S. Thomson, R. Borys, and D. C.

Rogers, 2003: Measurements of the concentration and composition of nuclei for cirrus formation. *Proc. Natl. Acad. Sci. USA*, **100**, 14 655–14 660, doi:10.1073/pnas.2532677100.

Ehrlich, A., E. Bierwirth, M. Wendisch, J. F. Gayet, G. Mioche, A. Lampert, and J. Heintzenberg, 2008: Cloud phase identification of Arctic boundary-layer clouds from airborne spectral reflection measurements: Test of three approaches. *Atmos. Chem. Phys.*, **8**, 7493–7505, doi:10.5194/acp-8-7493-2008.

Fahey, D. W., and Coauthors, 2014: The AquaVIT-1 intercomparison of atmospheric water vapor measurement techniques. *Atmos. Meas. Tech.*, **7**, 3177–3213, doi:10.5194/amt-7-3177-2014.

Gayet, J. F., and Coauthors, 2012a: On the observation of unusual high concentration of small chain-like aggregate ice crystals and large ice water contents near the top of a deep convective cloud during the CIRCLE-2 experiment. *Atmos. Chem. Phys.*, **12**, 727–744, doi:10.5194/acp-12-727-2012.

——, and Coauthors, 2012b: The evolution of microphysical and optical properties of an A380 contrail in the vortex phase. *Atmos. Chem. Phys.*, **12**, 6629–6643, doi:10.5194/acp-12-6629-2012.

Grooss, J. U., and Coauthors, 2005: Simulation of denitrification and ozone loss for the Arctic winter 2002/2003. *Atmos. Chem. Phys.*, **5**, 1437–1448, doi:10.5194/acp-5-1437-2005.

Groß, S., M. Wirth, A. Schäfler, A. Fix, S. Kaufmann, and C. Voigt, 2014: Potential of airborne lidar measurements for cirrus cloud studies. *Atmos. Meas. Tech.*, **7**, 2745–2755, doi:10.5194/amt-7-2745-2014.

Heymsfield, A. J., D. Baumgardner, P. DeMott, P. Forster, K. Gierens, and B. Kärcher 2010: Contrail microphysics. *Bull. Amer. Meteor. Soc.*, **91**, 465–469, doi:10.1175/2009BAMS2839.1.

——, and Coauthors, 2017: Cirrus clouds. *Ice Formation and Evolution in Clouds and Precipitation: Measurement and Modeling Challenges*, *Meteor. Monogr.*, doi:10.1175/AMSMONOGRAPHS-D-16-0010.1.

IPCC, 1999: *Summary for Policymakers: Aviation and the Global Atmosphere*. Cambridge University Press, 337 pp.

——, 2013: *Climate Change 2013: The Physical Science Basis*. Cambridge University Press, 1535 pp.

Iwabuchi, H., P. Yang, K. N. Liou, and P. Minnis, 2012: Physical and optical properties of persistent contrails: Climatology and interpretation. *J. Geophys. Res.*, **117**, D06215, doi:10.1029/2011JD017020.

Jackson, R. J., G. M. McFarquhar, A. M. Fridlind, and R. Atlas, 2015: The dependence of cirrus gamma size distributions expressed as volumes in N_0-λ-μ phase space and bulk cloud properties on environmental conditions: Results from the Small Ice Particles in Cirrus Experiment (SPARTICUS). *J. Geophys. Res. Atmos.*, **120**, 10 351–10 377, doi:10.1002/2015JD023492.

Jeßberger, P., and Coauthors, 2013: Aircraft type influence on contrail properties. *Atmos. Chem. Phys.*, **13**, 13 915–13 966, doi:10.5194/acpd-13-13915-2013.

Kärcher, B., and U. Lohmann, 2002: A parameterization of cirrus cloud formation: Homogeneous freezing of supercooled aerosols. *J. Geophys. Res.*, **107**, 4010, doi:10.1029/2001JD000470.

——, and J. Strom, 2003: The roles of dynamical variability and aerosols in cirrus cloud formation. *Atmos. Chem. Phys.*, **3**, 823–838, doi:10.5194/acp-3-823-2003.

Kaufmann, S., C. Voigt, P. Jeßberger, T. Jurkat, H. Schlager, A. Schwarzenboeck, M. Klingebiel, and T. Thornberry, 2014: In situ measurements of ice saturation in young contrails. *Geophys. Res. Lett.*, **41**, 702–709, doi:10.1002/2013GL058276.

——, and Coauthors, 2016: The airborne mass spectrometer AIMS—Part 1: AIMS-H_2O for UTLS water vapor measurements. *Atmos. Meas. Tech.*, **9**, 939–953, doi:10.5194/amt-9-939-2016.

Koop, T., B. Luo, A. Tsias, and T. Peter, 2000: Water activity as the determinant for homogeneous ice nucleation in aqueous solutions. *Nature*, **406**, 611–614, doi:10.1038/35020537.

Kox, S., L. Bugliaro, and A. Ostler, 2014: Retrieval of cirrus cloud optical thickness and top altitude from geostationary remote sensing. *Atmos. Meas. Tech.*, **7**, 3233–3246, doi:10.5194/amt-7-3233-2014.

Krämer, M., and Coauthors, 2009: Ice supersaturation and cirrus cloud crystal numbers. *Atmos. Chem. Phys.*, **9**, 3505–3522, doi:10.5194/acp-9-3505-2009.

——, and Coauthors, 2016: A microphysics guide to cirrus clouds—Part 1: Cirrus types. *Atmos. Chem. Phys.*, **16**, 3463–3483, doi:10.5194/acp-16-3463-2016.

Lawson, R. P., B. Baker, B. Pilson, and Q. X. Mo, 2006: In situ observations of the microphysical properties of wave, cirrus, and anvil clouds. Part II: Cirrus clouds. *J. Atmos. Sci.*, **63**, 3186–3203, doi:10.1175/JAS3803.1.

Lee, D. S., D. W. Fahey, P. M. Forster, P. J. Newton, R. C. N. Wit, L. L. Lim, B. Owen, and R. Sausen, 2009: Aviation and global climate change in the 21st century. *Atmos. Environ.*, **43**, 3520–3537, doi:10.1016/j.atmosenv.2009.04.024.

Lewellen, D. C., 2014: Persistent contrails and contrail cirrus. Part II: Full lifetime behavior. *J. Atmos. Sci.*, **71**, 4420–4438, doi:10.1175/JAS-D-13-0317.1.

Liou, K. N., 1986: Influence of cirrus clouds on weather and climate processes: A global perspective. *Mon. Wea. Rev.*, **114**, 1167–1199, doi:10.1175/1520-0493(1986)114<1167:IOCCOW>2.0.CO;2.

Luebke, A. E., and Coauthors, 2016: The origin of midlatitude ice clouds and the resulting influence on their microphysical properties. *Atmos. Chem. Phys.*, **16**, 5793–5809, doi:10.5194/acp-16-5793-2016.

Madonna, E., H. Wernli, H. Joos, and O. Martius, 2014: Warm conveyor belts in the ERA-Interim dataset (1979–2010). Part I: Climatology and potential vorticity evolution. *J. Climate*, **27**, 3–26, doi:10.1175/JCLI-D-12-00720.1.

Meyer, J., and Coauthors, 2015: Two decades of water vapor measurements with the FISH fluorescence hygrometer: A review. *Atmos. Chem. Phys.*, **15**, 8521–8538, doi:10.5194/acp-15-8521-2015.

Minikin, A., A. Petzold, J. Strom, R. Krejci, M. Seifert, P. van Velthoven, H. Schlager, and U. Schumann, 2003: Aircraft observations of the upper tropospheric fine particle aerosol in the Northern and Southern Hemispheres at midlatitudes. *Geophys. Res. Lett.*, **30**, 1503, doi:10.1029/2002GL016458.

Minnis, P., and Coauthors, 2013: Linear contrail and contrail cirrus properties determined from satellite data. *Geophys. Res. Lett.*, **40**, 3220–3226, doi:10.1002/grl.50569.

Muhlbauer, A., T. P. Ackerman, J. M. Comstock, G. S. Diskin, S. M. Evans, R. P. Lawson, and R. T. Marchand, 2014: Impact of large-scale dynamics on the microphysical properties of midlatitude cirrus. *J. Geophys. Res. Atmos.*, **119**, 3976–3996, doi:10.1002/2013JD020035.

Murphy, D. M., and T. Koop, 2005: Review of the vapour pressures of ice and supercooled water for atmospheric applications. *Quart. J. Roy. Meteor. Soc.*, **131**, 1539–1565, doi:10.1256/qj.04.94.

Ovarlez, J., J. F. Gayet, K. Gierens, J. Strom, H. Ovarlez, F. Auriol, R. Busen, and U. Schumann, 2002: Water vapour measurements inside cirrus clouds in Northern and Southern Hemispheres during INCA. *Geophys. Res. Lett.*, **29**, doi:10.1029/2001GL014440.

Petzold, A., and Coauthors, 1997: Near-field measurements on contrail properties from fuels with different sulfur content. *J. Geophys. Res.*, **102**, 29 867–29 880, doi:10.1029/97JD02209.

Prados-Roman, C., and Coauthors, 2011: Airborne DOAS limb measurements of tropospheric trace gas profiles: Case studies on the profile retrieval of O_4 and BrO. *Atmos. Meas. Tech.*, **4**, 1241–1260, doi:10.5194/amt-4-1241-2011.

Rautenhaus, M., G. Bauer, and A. Dörnbrack, 2012: A web service based tool to plan atmospheric research flights. *Geosci. Model Dev.*, **5**, 55–71, doi:10.5194/gmd-5-55-2012.

Schäfler, A., M. Boettcher, C. M. Grams, M. Rautenhaus, H. Sodemann, and H. Wernli, 2014: Planning aircraft measurements within a warm conveyor belt. *Weather*, **69**, 161–166, doi:10.1002/wea.2245.

Schiller, C., M. Krämer, A. Afchine, N. Spelten, and N. Sitnikov, 2008: Ice water content of Arctic, midlatitude, and tropical cirrus. *J. Geophys. Res.*, **113**, D24208, doi:10.1029/2008JD010342.

Schmetz, J., P. Pili, S. Tjemkes, D. Just, J. Kerkmann, S. Rota, and A. Ratier, 2002: An introduction to Meteosat Second Generation (MSG). *Bull. Amer. Meteor. Soc.*, **83**, 977–987, doi:10.1175/1520-0477(2002)083<0977:AITMSG>2.3.CO;2.

Schnaiter, M., and Coauthors, 2016: Cloud chamber experiments on the origin of ice crystal complexity in cirrus clouds. *Atmos. Chem. Phys.*, **16**, 5091–5110, doi:10.5194/acp-16-5091-2016.

Schröder, F., B. Kärcher, C. Duroure, J. Strom, A. Petzold, J. F. Gayet, B. Strauss, P. Wendling, and S. Borrmann, 2000: On the transition of contrails into cirrus clouds. *J. Atmos. Sci.*, **57**, 464–480, doi:10.1175/1520-0469(2000)057<0464:OTTOCI>2.0.CO;2.

Schumann, U., 2012: A contrail cirrus prediction model. *Geosci. Model Dev.*, **5**, 543–580, doi:10.5194/gmd-5-543-2012.

——, and K. Graf, 2013: Aviation-induced cirrus and radiation changes at diurnal timescales. *J. Geophys. Res. Atmos.*, **118**, 2404–2421, doi:10.1002/jgrd.50184.

——, H. Schlager, F. Arnold, R. Baumann, P. Haschberger, and O. Klemm, 1998: Dilution of aircraft exhaust plumes at cruise altitudes. *Atmos. Environ.*, **32**, 3097–3103, doi:10.1016/S1352-2310(97)00455-X.

——, B. Mayer, K. Gierens, S. Unterstrasser, P. Jessberger, A. Petzold, C. Voigt, and J. F. Gayet, 2011: Effective radius of ice particles in cirrus and contrails. *J. Atmos. Sci.*, **68**, 300–321, doi:10.1175/2010JAS3562.1.

——, ——, K. Graf, and H. Mannstein, 2012: A parametric radiative forcing model for contrail cirrus. *J. Appl. Meteor. Climatol.*, **51**, 1391–1406, doi:10.1175/JAMC-D-11-0242.1.

——, J. E. Penner, Y. B. Chen, C. Zhou, and K. Graf, 2015: Dehydration effects from contrails in a coupled contrail-climate model. *Atmos. Chem. Phys.*, **15**, 11 179–11 199, doi:10.5194/acp-15-11179-2015.

——, and Coauthors, 2017: Properties of individual contrails: a compilation of observations and some comparisons. *Atmos. Chem. Phys.*, **17**, 403–438, doi:10.5194/acp-17-403-2017.

Spichtinger, P., and K. M. Gierens, 2009a: Modelling of cirrus clouds—Part 2: Competition of different nucleation mechanisms. *Atmos. Chem. Phys.*, **9**, 2319–2334, doi:10.5194/acp-9-2319-2009.

——, and ——, 2009b: Modelling of cirrus clouds—Part 1a: Model description and validation. *Atmos. Chem. Phys.*, **9**, 685–706, doi:10.5194/acp-9-685-2009.

——, ——, and H. Wernli, 2005: A case study on the formation and evolution of ice supersaturation in the vicinity of a warm conveyor belt's outflow region. *Atmos. Chem. Phys.*, **5**, 973–987, doi:10.5194/acp-5-973-2005.

Sprenger, M., and H. Wernli, 2015: The LAGRANTO Lagrangian analysis tool—Version 2.0. *Geosci. Model Dev.*, **8**, 2569–2586, doi:10.5194/gmd-8-2569-2015.

Stevens, B., and S. Bony, 2013: What are climate models missing? *Science*, **340**, 1053–1054, doi:10.1126/science.1237554.

Stith, J. L., and Coauthors, 2014: Ice particles in the upper anvil regions of midlatitude continental thunderstorms: The case for frozen-drop aggregates. *Atmos. Chem. Phys.*, **14**, 1973–1985, doi:10.5194/acp-14-1973-2014.

Trenberth, K. E., and Coauthors, 2007: Observations: Surface and atmospheric climate change. *Climate Change 2007: The Physical Science Basis*, S. Solomon et al., Eds., Cambridge University Press, 235–336.

Vali, G., P. J. DeMott, O. Mohler, and T. F. Whale, 2015: Technical note: A proposal for ice nucleation terminology. *Atmos. Chem. Phys.*, **15**, 10 263–10 270, doi:10.5194/acp-15-10263-2015.

Vazquez-Navarro, M., H. Mannstein, and S. Kox, 2015: Contrail life cycle and properties from 1 year of MSG/SEVIRI rapid-scan images. *Atmos. Chem. Phys.*, **15**, 8739–8749, doi:10.5194/acp-15-8739-2015.

Voigt, C., and Coauthors, 2006: Nitric acid in cirrus clouds. *Geophys. Res. Lett.*, **33**, L05803, doi:10.1029/2005GL025159.

——, and Coauthors, 2010: In-situ observations of young contrails—Overview and selected results from the CONCERT campaign. *Atmos. Chem. Phys.*, **10**, 9039–9056, doi:10.5194/acp-10-9039-2010.

——, and Coauthors, 2011: Extinction and optical depth of contrails. *Geophys. Res. Lett.*, **38**, L11806, doi:10.1029/2011GL047189.

——, and Coauthors, 2014: Evolution of CO_2, SO_2, HCl, and HNO_3 in the volcanic plumes from Etna. *Geophys. Res. Lett.*, **41**, 2196–2203, doi:10.1002/2013GL058974.

Wang, Z., and K. Sassen, 2002: Cirrus cloud microphysical property retrieval using lidar and radar measurements. Part II: Midlatitude cirrus microphysical and radiative properties. *J. Atmos. Sci.*, **59**, 2291–2302, doi:10.1175/1520-0469(2002)059<2291:CCMPRU>2.0.CO;2.

Weidner, F., and Coauthors, 2005: Balloon-borne limb profiling of UV/vis skylight radiances, O_3, NO_2, and BrO: Technical set-up and validation of the method. *Atmos. Chem. Phys.*, **5**, 1409–1422, doi:10.5194/acp-5-1409-2005.

Weigel, R., and Coauthors, 2016: Thermodynamic correction of particle concentrations measured by underwing probes on fast flying aircraft. *Atmos. Meas. Tech.*, **9**, 5135–5162, doi:10.5194/amt-9-5135-2016.

Wendisch, M., P. Yang, and P. Pilewskie, 2007: Effects of ice crystal habit on thermal infrared radiative properties and forcing of cirrus. *J. Geophys. Res.*, **112**, D08201, doi:10.1029/2006JD007899.

——, and Coauthors, 2016: ACRIDICON–CHUVA campaign: Studying tropical deep convective clouds and precipitation over Amazonia using the new German research aircraft HALO. *Bull. Amer. Meteor. Soc.*, **97**, 1885–1908, doi:10.1175/BAMS-D-14-00255.1.

Wernli, H., M. Boettcher, H. Joos, A. K. Miltenberger, and P. Spichtinger, 2016: A trajectory-based classification of ERA-Interim ice clouds in the region of the North Atlantic storm track. *Geophys. Res. Lett.*, **43**, 6657–6664, doi:10.1002/2016GL068922.

Winker, D. M., and Coauthors, 2010: The *CALIPSO* mission: A global 3D view of aerosols and clouds. *Bull. Amer. Meteor. Soc.*, **91**, 1211–1229, doi:10.1175/2010BAMS3009.1.

Wirth, M., A. Fix, P. Mahnke, H. Schwarzer, F. Schrandt, and G. Ehret, 2009: The airborne multi-wavelength water vapor differential absorption lidar WALES: System design and performance. *Appl. Phys.*, **96B**, 201–213, doi:10.1007/s00340-009-3365-7.

Wylie, D. P., and W. P. Menzel, 1999: Eight years of high cloud statistics using HIRS. *J. Climate*, **12**, 170–184, doi:10.1175/1520-0442-12.1.170.

Yang, H. Y., S. Dobbie, R. Herbert, P. Connolly, M. Gallagher, S. Ghosh, S. Al-Jumur, and J. Clayton, 2012: The effect of observed vertical structure, habits, and size distributions on the solar radiative properties and cloud evolution of cirrus clouds. *Quart. J. Roy. Meteor. Soc.*, **138**, 1221–1232, doi:10.1002/qj.973.

Zahn, A., J. Weppner, H. Widmann, K. Schlote-Holubek, B. Burger, T. Kuhner, and H. Franke, 2012: A fast and precise chemiluminescence ozone detector for eddy flux and airborne application. *Atmos. Meas. Tech.*, **5**, 363–375, doi:10.5194/amt-5-363-2012.

Zhang, Y., A. Macke, and F. Albers, 1999: Effect of crystal size spectrum and crystal shape on stratiform cirrus radiative forcing. *Atmos. Res.*, **52**, 59–75, doi:10.1016/S0169-8095(99)00026-5.

Ziereis, H., H. Schlager, P. Schulte, P. F. J. van Velthoven, and F. Slemr, 2000: Distributions of NO, NO*x*, and NO*y* in the upper troposphere and lower stratosphere between 28° and 61°N during POLINAT 2. *J. Geophys. Res.*, **105**, 3653–3664, doi:10.1029/1999JD900870.

Zöger, M., and Coauthors, 1999: Fast in situ stratospheric hygrometers: A new family of balloon-borne and airborne Lyman alpha photofragment fluorescence hygrometers. *J. Geophys. Res.*, **104**, 1807–1816, doi:10.1029/1998JD100025.